THE JOURNAL OF PHYSICAL CHEMISTRY C
A JOURNAL OF THE AMERICAN CHEMICAL SOCIETY

pubs.acs.org/JPCC

Article

Local Order in Liquid Gallium–Indium Alloys

Alfred Amon,* Philip A. Chater, Gavin Vaughan, Rachael Smith, and Christoph G. Salzmann

Cite This: J. Phys. Chem. C 2023, 127, 16687–16694

Read Online

ACCESS | Metrics & More | Article Recommendations | Supporting Information

ABSTRACT: Liquid metals such as eutectic Ga–In alloys have low melting points and low toxicity and are used in catalysis and micro-robotics. This study investigates the local atomic structure of liquid gallium-indium alloys by a combination of density measurements, diffraction data, and Monte-Carlo simulation via the empirical potential structure refinement approach. A high-Q shoulder observed in liquid Ga is related to structural rearrangements in the second coordination shell. Structure analysis found coordination environments close to a random distribution for eutectic Ga–In alloy, while electronic effects appear to dominate the mixing enthalpy.

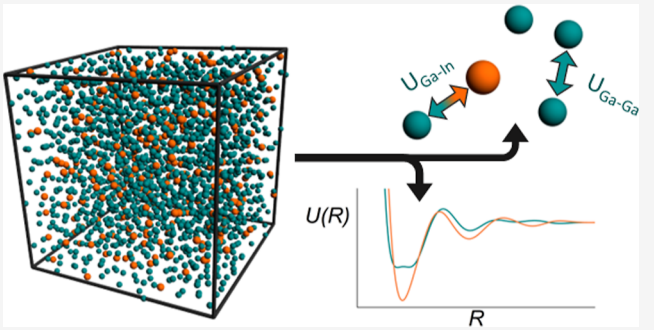

INTRODUCTION

Sitting at the border between transition-metal and metalloid elements, gallium displays one of the most puzzling structural chemistries among the elements. The complex crystal structure of its room temperature stable modification α-Ga features gallium dimers with mixed covalent and metallic bonding character.[1] Here, every atom is coordinated by one neighbor at a covalent bonding distance of d_{Ga-Ga} = 2.48 Å and six neighbors at a larger distance (>2.7 Å). Also, the metastable and high-pressure allotropes form structure types uncommon for metallic elements.[2] Due to its non-close-packed crystal structure, α-Ga experiences a 3% density increase upon melting, with a concomitant increase of coordination number (CN) from 1 + 6 to about 11.[3,4] Speculations about the persistence of Ga_2 pairs[5] or larger clusters[6,7] upon melting of the α-Ga modification initiated investigations of the liquid structure in an attempt to explain the characteristic high-Q shoulder observed on the first diffraction peak.[8,9] This shoulder is even more pronounced in the supercooled liquid[10] and resolved as a separate peak in amorphous gallium films (CN = 9.3).[11] Besides covalent Ga–Ga bonds in the first coordination shell, rearrangements in the second shell, due to the influence of medium-range Friedel oscillations, have been held responsible for the structural anomalies.[9] Its anomalous properties sustain ongoing interest to understand the structure of liquid gallium.

Room-temperature liquid alloys, also known as liquid metals, typically have liquidus temperatures below 300 °C and are based on the low-melting elements gallium, bismuth, indium, cesium, sodium, and mercury as majority components.[12] More recently, liquid metals were discovered as heterogeneous catalysts with the renewable surface for CO_2 reduction[13,14] or petrol refining,[15] templates for synthesis of 2D-materials,[16] for tailored growth of microcrystals[17] and as electrode material in all-liquid batteries.[18,19] In particular, gallium alloys display low-melting points, wide liquid range, low toxicity, and chemical inertness making them suitable as liquid-metal inks for flexible printed electronics[20,21] or as pumps and actuators in microfluidic devices.[22−25] A suspension of magnetic particles in liquid gallium can function as a shape-shifting miniature machine with field-assisted solid–liquid transition.[26]

Like the pure element, hypoeutectic gallium alloys display strong undercooling[27] and in particular the low melting binary eutectic $Ga_{0.858}In_{0.142}$ (liquidus temperature T_{liq} = 15 °C) and the ternary eutectic $Ga_{78.3}In_{14.9}Sn_{6.8}$ (T_{liq} = 13.2 °C), known as "Galinstan" are of technological interest.[12] Early X-ray scattering studies of liquid Ga–In alloys found a rapid increase of the nearest-neighbor interatomic distance in the pair correlation function with rising indium content, which flattens out above 50 at. % In and a maximum of the first shell coordination number (CN_{avg} ≈ 12.3) around the equiatomic composition, showing little temperature dependence.[28] Ding et al. postulated the appearance of clusters reminiscent of crystalline structures for alloys greater 30 at. % In.[29] The pressure-induced crystallization of liquid $Ga_{86}In_{14}$ above 3.4 GPa was studied by X-ray diffraction and molecular dynamic simulations.[30,31] Around 400 K, a discontinuous change in coordination number was observed in the binary eutectic composition and interpreted as a rearrangement in the first and second coordination shell.[32] Zhao and co-workers investigated the melt fragility of supercooled Ga–In melts by X-ray

Received: June 7, 2023
Revised: July 27, 2023
Published: August 9, 2023

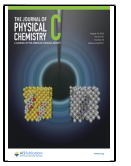

https://doi.org/10.1021/acs.jpcc.3c03857
J. Phys. Chem. C 2023, 127, 16687–16694

absorption spectroscopy, diffraction, and viscosimetry, observing distinct changes in the viscosity below the liquidus temperature and suggesting the presence of low-coordinated polyhedra in the supercooled liquid.[33,34] A combination of synchrotron X-ray diffraction and ab-initio molecular dynamics simulations, however, observed no abnormal structural changes upon supercooling of Ga−In eutectic alloy.[31]

Experimental phase diagram studies and thermodynamic measurements in liquid Ga−In system indicate near regular solution behavior.[35−44] The parabolic trend of the mixing enthalpy with a maximum of +1.1 kJ mol^{-1} at the equiatomic composition indicates preferred homoatomic interactions in the liquid.[41] Having a metallic radius difference around 18%, alloys of the isoelectronic elements gallium and indium are just above the Hume-Rothery solubility criterion,[45] as evidenced by complete miscibility in the liquid phase but asymmetric miscibility in the solid (Figure 1A). Around 50 at. % In, the Ga−In phase diagram (Figure 1A) features a flattened liquidus slope, which can be related to the positive mixing enthalpy in the liquid phase.[46,47]

In this study, we have collected density measurements, synchrotron, and neutron diffraction data combined with Monte-Carlo-based empirical potential structure refinements (EPSR) to study the structure of liquid Ga−In alloys. In particular, we aim to understand (i) the origin of the high-Q shoulder on the first diffraction peak of liquid gallium; (ii) whether liquid Ga−In alloys can be treated as ideal solutions; and (iii) if are there preferred atomic interactions leading to the suggested demixing tendencies.

METHODS

Sample handling was carried out in a glovebox system with a nitrogen atmosphere (pO_2 < 0.5 ppm). Liquid alloy samples were prepared by combining stoichiometric amounts of gallium (Acros, 99.99%) and indium (Aldrich, 99.99%) in glass vials and heating for 1 h to 200 °C to ensure homogenization.

Density Measurements. Density measurements were performed in a borosilicate glass pycnometer after Guy-Lussac (approx. 1 cm^3 inner volume). The pycnometer was calibrated at 200 °C with pure gallium (reported density of ρ(200 °C) = 5.9737(18) g cm^{-3}[48]). Density data are therefore given with respect to this value. The pycnometer (flask and capillary plug) was weighed at room temperature in an empty state, filled with about 0.8 cm^3 of liquid alloy sample, and weighed. The residual volume was filled with degassed silicone oil (oil bath grade). The filled pycnometer flask and capillary plug were heated and equilibrated at T = 200 °C ± 3 °C. The capillary plug was inserted at 200 °C and the expelled excess silicone oil was removed. Then, the cooled-down pycnometer was weighed again to correct the contribution of the silicon oil. The volumetric mass density is reported as the mean value and estimated standard deviation from three independent measurements per sample composition.

X-ray Diffraction. X-ray diffraction experiments for temperatures of 150 °C and below were conducted at the ID15A beamline of the ESRF (Grenoble, France) using a wavelength λ = 0.125234(1) Å with a Dectris Pilatus3X-CdTe-2M detector.[70] X-ray diffraction experiments at 200 °C were conducted at the I15-1 beamline of the Diamond Light source (Rutherford-Appleton Laboratory, Didcot, United Kingdom) λ = 0.16167(1) Å. Liquid alloy samples were contained in fused silica capillaries and heated using a hot gas blower. Data

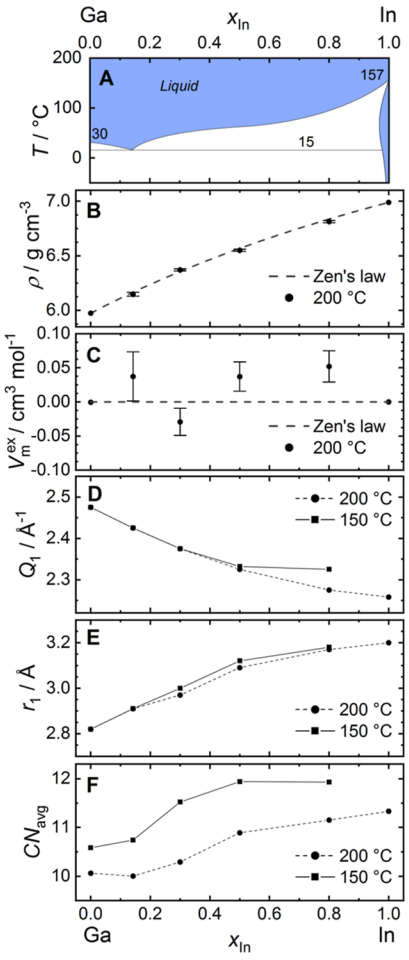

Figure 1. Selected physical properties of the Ga−In system. (A) Reported phase diagram reproduced with data from ref 35. Numbers in the figure indicate the melting points of pure elements and the eutectic temperature. Experimental values for (B) volumetric mass density ρ, and (C) derived molar excess volumes V_m^{ex} at T = 200 °C. (D) Position of the first maximum Q_1 in the total structure factor $S(Q)$ and (E) position of the first maximum r_1 in $G(r)$. (F) Average coordination number CN_{avg} in the first coordination shell. Lines in (D−F) are guides to the eye. Error bars indicate one e.s.d.

reduction, normalization, and correction for furnace and capillary background contributions, beam polarization, attenuation effects, and multiple scattering were done using the DAWN[71] and GudrunX[72] software packages.

Time-of-Flight Neutron Diffraction. Time-of-flight neutron diffraction data were collected on the GEM beamline of the ISIS spallation source (Rutherford-Appleton Laboratory, Didcot, UK). Samples were measured in fused silica ampoules of 10 mm outer diameter and 1 mm wall thickness. Alloys with higher indium content were not accessible to neutron diffraction, due to the strong neutron absorption by indium. Only the time-of-flight data below a neutron energy of 0.33 eV were used to avoid the strong neutron resonance of indium.[73] Further details on data collection and correction can be found in ref 74. For the EPSR analysis of liquid Ga and $Ga_{0.858}In_{0.142}$, simulation boxes containing 1000 Ga atoms, and 1716 Ga plus 284 In atoms, respectively, were constructed according to experimental densities. After structure randomization, the structure model was refined to energy convergence employing only set Lennard-Jones potentials. The Lennard-Jones distance

https://doi.org/10.1021/acs.jpcc.3c03857
J. Phys. Chem. C 2023, 127, 16687−16694

parameters σ were selected according to atomic radii and then iterated to get the best possible agreement with experimental data. Then, the maximum amplitude for the empirical potentials was increased in steps of 0.5 kJ mol^{-1} until no further improvement of the model was achievable. For the final analysis, 3000 or more simulation snapshots were accumulated and the ensemble was averaged.

RESULTS AND DISCUSSION

The volumetric mass density ρ of the liquid $Ga_{1-x}In_x$ alloys (x_{In} = 0.0, 0.142, 0.3, 0.5, 0.8, 1.0) at T = 200 °C ranges from ρ = 5.974(2) g cm^{-3}[48] for pure gallium to ρ = 6.99(1) g cm^{-3} for pure indium and exhibits a nonlinear change with composition (Figure 1B, Table S1). Zen's law predicts a linear change in molar volume for ideal solutions, corresponding to constant partial molar volumes, which results in a nonlinear function for the volumetric mass density.[49] The slight positive deviation from linear behavior of the experimental density values is in excellent agreement with the theoretical density (dashed line in Figure 1B) corresponding to linear behavior of the composition averaged molar volume. The derived values for the molar excess volumes V_m^{ex} show no significant deviation from ideality within experimental error (Figure 1C) and did not show the irregular behavior observed by Ben Shalom et al.[39]

To investigate the local order in liquid gallium−indium alloys, synchrotron X-ray diffraction data were collected for the composition series at T = 150 and 200 °C. Additionally, neutron time-of-flight data were collected at T = 150 °C for pure gallium and the eutectic composition $Ga_{0.858}In_{0.142}$. The high neutron absorption cross section of indium precluded neutron diffraction studies at higher indium content.[50] At 200 °C, the total scattering structure factor $S(Q)$ for the series of alloys (Figure 2A) displays a broad first peak, characteristic for liquid alloys with a peak maximum located in the range Q_1 = 2.6−2.8 Å^{-1}, followed by rapidly decaying oscillations at higher Q values. Above Q = 12 Å^{-1}, the structure factor becomes featureless. For the intermediate compositions x_{In} = 0.3 and x_{In} = 0.5, the oscillations in $S(Q)$ appear to be dampened faster, indicating more structural disorder. The structure factor for pure liquid gallium (x_{In} = 0.0) displays a distinct high-Q shoulder on the first peak, which becomes less pronounced with increasing indium content. With increasing indium content, the position of the first maximum Q_1 shifts gradually to lower Q as gallium atoms are substituted by the larger indium atoms, increasing the average nearest neighbor distance between atoms (Figure 1D). The values for Q_1 at 150 and 200 °C differ only at high indium content.

The total pair distribution functions $G(r)$ for the series of liquid Ga−In alloys at T = 200 °C (Figure 2B) were obtained by Fourier transform of the respective structure factors. Below r = 2.5 Å, $G(r)$ shows irregular oscillations around zero due to Fourier truncation artifacts. The first peak in $G(r)$ corresponds to the average interatomic distance in the first coordination shell and the position of the peak maximum r_1 increases from r_1 = 2.82 Å for x_{In} = 0.0 to r_1 = 3.20 Å for x_{In} = 1.0 (Figure 1E). These values follow the metallic radii of gallium (1.4 Å) and indium (1.7 Å).[51] At low indium concentration, the values for r_1 increase linearly with In content but flatten out above x_{In} = 0.5.

The position of the first diffraction peak scaled by the mean atomic diameter Q_1r_1 has been used as a classifier of order in amorphous solids and liquids.[52] Topological order such as in hard-sphere liquids originates from the closest approach of neighboring atoms due to the short-range repulsive potential and yields a strong peak in $G(r)$ with r_1 close to the mean atomic diameter and we find values of $Q_1r_1 \approx 5\pi/2 \approx 7.5$. Materials with additional chemical order due to Coulomb repulsion or directional bonding typically display values for Q_1r_1 around 4.5 or 2.5, respectively.[53] For the investigated liquid $Ga_{1-x}In_x$ alloys, Q_1r_1 lies in the range 6.9−7.4 indicating that topological order due to size effects is prevalent (cf. Figure S2).

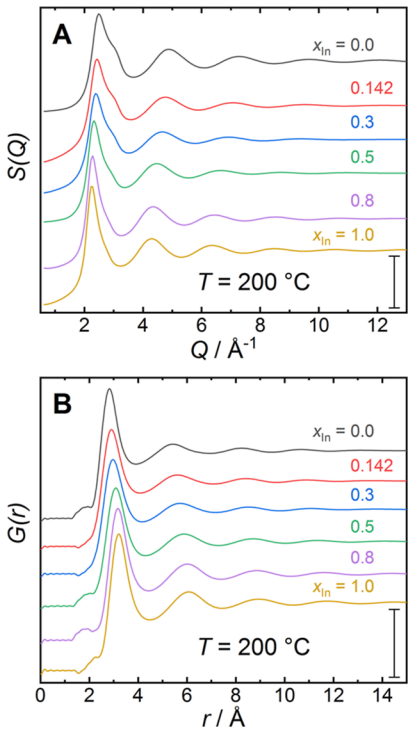

Figure 2. (A) Total X-ray structure factors $S(Q)$ and (B) the derived pair distribution functions $G(r)$ for the investigated series of liquid Ga−In alloys at T = 200 °C as obtained from X-ray diffraction data. Curves are shifted vertically for clarity. Scale bars in (A) and (B) represent a unit of one in $S(Q)$ and $G(r)$, respectively.

The average coordination number CN_{avg} in the first shell was obtained by integration of the radial distribution function $T(r) = 4\pi\rho_0 r^2 G(r)$ up to the first minimum in $T(r)$, where ρ_0 is the number density. At T = 200 °C, a coordination number of CN_{avg} = 10.1(2) was obtained for pure gallium (x_{In} = 0.0). Initially, CN_{avg} remains nearly unchanged at 10.3(2) for the eutectic composition (x_{In} = 0.142) and then shows a strong increase to CN_{avg} = 10.9(1) for x_{In} = 0.5 (cf. Figure 1F). In the range x_{In} = 0.5−1.0, the CN_{avg} increases slowly to the maximum of CN_{avg} = 11.3(2) for pure indium. Data for CN_{avg} at T = 150 °C show a similar trend with a more pronounced step, increasing from 10.6(1) for liquid gallium to 11.9(2) for x_{In} = 0.8.

A similar trend of $Q_1(x_{In})$, $r_1(x_{In})$, and $CN_{avg}(x_{In})$ was also reported by Gebhardt[28] and Vahvaselkä,[54] who observed the change in slope around 50 at. % In and 30 at. % In, respectively. Gebhardt interpreted this observation within a micro-inhomogeneous segregation model, where two preferred local environments are present in the liquid.[28] We used the EPSR method to create an atomistic model reproducing the experimental diffraction data of the liquid alloys and extract the partial pair distribution functions. The EPSR methodology is a

https://doi.org/10.1021/acs.jpcc.3c03857
J. Phys. Chem. C 2023, 127, 16687−16694

Monte-Carlo simulation method where experimental diffraction data are used in combination with prior chemical information (density, pair potentials) to refine an atomistic model that describes the diffraction data.[55,56] To improve the description of the diffraction data, empirical potentials are employed which correct the initial Lennard-Jones pair potentials to better describe the experiment. Neutron time-of-flight diffraction data were collected on the GEM diffractometer (RAL-ISIS, UK) to complement the X-ray diffraction data and examine the short-range order in liquid gallium and the liquid gallium-indium eutectic alloy (x_{In} = 0.142) in more detail. For the binary alloy $Ga_{0.858}In_{0.142}$, the additional scattering contrast yields more detailed information on the partial pair distribution functions $G_{ij}(r)$ and the dominant interactions in this liquid alloy system.

A simulation box containing 1000 gallium atoms was used to model liquid gallium at 150 °C. The converged structural model using an interatomic Lennard-Jones 12−6 potential (σ = 2.7 Å, ε = 1.8 kJ mol^{-1}) was able to reproduce the general trend of $S(Q)$ and the corresponding pair distribution function $G(r)$ for pure gallium (Figure 3). However, this model could

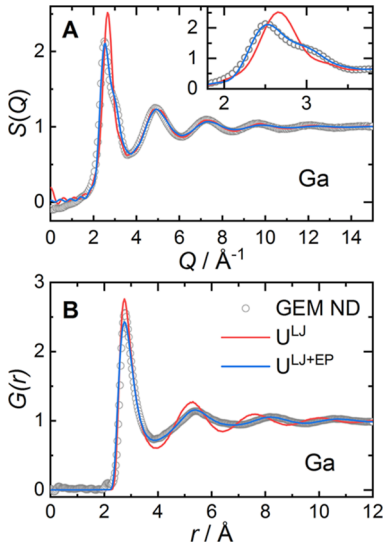

Figure 3. (A) Total structure factor $S(Q)$ and (B) corresponding pair distribution function $G(r)$ for liquid gallium at T = 150 °C obtained from neutron diffraction data on the GEM beamline (open circles). The simulated $S(Q)$ and $G(r)$ using only the Lennard-Jones potential U^{LJ} and using also the empirical potential U^{LJ+EP} are given as solid lines. Figure legend in panel B.

not reproduce the high-Q shoulder on the first diffraction peak in $S(Q)$. The first coordination shell in $G(r)$ appears well described but at larger distances the discrepancies grow. To improve the agreement between experimental and simulated structure factors, an empirical potential U^{EP} was introduced additionally to the initial Lennard-Jones potential U^{LJ} (details of the procedure are given in ref 55 56,). Using the converged total potential U^{LJ+EP} improved the description of the first diffraction peak and the experimental pair distribution function. The refined empirical potential (Figure 4A) has a first minimum at r = 3.72 Å, followed by a dampened oscillatory behavior with minima at r = 6.39 Å (well depth ε = −0.57 kJ mol^{-1}) and r = 8.85 Å (ε = −0.03 kJ mol^{-1}). The total potential U^{LJ+EP} displays a strongly broadened minimum centered on r = 3.42 Å (ε = −2.87 kJ mol^{-1}) and a second

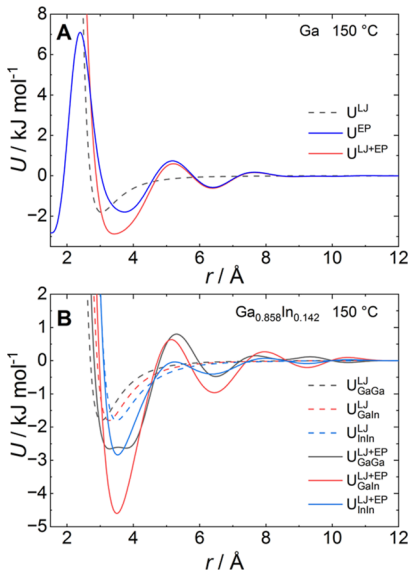

Figure 4. (A) Lennard-Jones potential U^{LJ}, final empirical potential U^{EP}, and resulting total potential U^{LJ+EP} for liquid gallium at T = 150 °C. (B) Final pair potentials for the EPSR model of the liquid eutectic $Ga_{0.858}In_{0.142}$ alloy at 150 °C. Lennard-Jones potentials U^{LJ} (dashed lines) and final total potentials U^{LJ+EP} (solid lines).

minimum of the pair potential located approximately 1 Å beyond the second maximum in $G(r)$ at r = 5.4. The modified potential U^{LJ+EP} reduces the coordination number in the first shell from 11.7(1) to 10.6(1) but yields an improved description of the second and third coordination shells which are spread out to larger distances (Figure 3B). The structure model using the converged empirical potential can reproduce the characteristic shoulder on the first diffraction peak and suggests that the corresponding structural rearrangements occur not in the first but in the second and third coordination shells, similar to the simulation results of Tsai and co-workers.[9]

Here, a discussion of the refined empirical potential $U(r)^{EP}$ with regard to the postulated interatomic pair potentials due to Friedel-type charge density oscillations is appropriate. Friedel oscillations are dampened oscillations in the interaction potential of liquid metals $U(r)$ which originate from a discontinuity in the dielectric constant $\varepsilon(k)$ of the electron gas k = 2 k_F, where k_F is the Fermi momentum (for liquid gallium $k_F \approx$ 1.65 Å^{-1}).[57,58] In real space, this results in oscillations in the charge density and the pair potential with periodicity 2 k_F.[59] The radial spacing of the minima in the converged potential for gallium $U(r)^{LJ+EP}$ is about 1.3 Å and does not coincide with the predicted wavelength of Friedel oscillations of $\lambda_F = 2\pi/2\ k_F$ = 1.92 Å in the long-range limit.[59]

Another point to consider is that while the use of the refined empirical potential led to a vastly improved description of the experimental data by the obtained atomistic model, the well depth of the second minimum in the interatomic potential U^{LJ+EP} is only −0.57 kJ mol^{-1}, i.e., about 20% of the first minimum and only about 16% of the estimated thermal energy k_BT at T = 150 °C.[60] Most likely, the influence of the empirical potential lies therefore less with the second and third minima, but with the steep and pronounced maximum in $U(r)^{LJ+EP}$ at r ≈ 5.2 Å, which pushes the second coordination shell outwards beyond the hard-sphere result and leads to the medium-range order responsible for the high-Q shoulder on the first diffraction peak. The static structure factor $S(Q)$ for liquid

https://doi.org/10.1021/acs.jpcc.3c03857
J. Phys. Chem. C 2023, 127, 16687−16694

indium at 200 °C (Figure S4) does not display a high-Q shoulder on the first diffraction peak (cf. ref S4), but is well described by the Percus−Yevick structure factor for a hard-sphere liquid with radius σ = 1.476 Å and packing fraction φ = 0.42.[61−63]

For one-component systems, such as pure gallium, a single diffraction contrast suffices to obtain the complete pair distribution function. For the two-component system $Ga_{0.858}In_{0.142}$, three data sets of dissimilar diffraction contrast are necessary to completely determine the three partial structure factors $S_{ij}(Q)$ (i,j = Ga, In) and corresponding partial pair distribution functions $G_{ij}(r)$. The atomistic model for the eutectic $Ga_{0.858}In_{0.142}$ was refined against both, X-ray synchrotron and neutron diffraction data. The introduction of physical constraints in the EPSR model alleviates the lack of a third diffraction contrast. The model using only Lennard-Jones potentials (σ_{Ga} = 2.70 Å, ε_{Ga} = 1.80 kJ mol^{-1}, σ_{In} = 3.11 Å, ε_{In} = 1.80 kJ mol^{-1}) shows approximate agreement with the experimental data. The amplitude of the empirical potential U^{EP} was then increased in small steps from 0 to 4 kJ mol^{-1} until no further improvement in the fit between experimental and simulated diffraction data was achieved (Figure S6). As for liquid gallium, the refined interatomic potentials $U(r)^{LJ+EP}$ show a deep first minimum for all atom pairs, followed by oscillatory decay at larger distances (Figure 4B). The interaction between gallium and indium $U^{LJ+EP}_{GaIn(r)}$ has a particularly deep first minimum, while the gallium−gallium interaction $U^{LJ+EP}_{GaGa(r)}$ shows a strongly broadened minimum. From the atomistic model, the Faber−Ziman partial pair distribution functions G^{FZ}_{ij} and their respective Fourier transforms S^{FZ}_{ij} (Figure 5) were calculated. Examination of

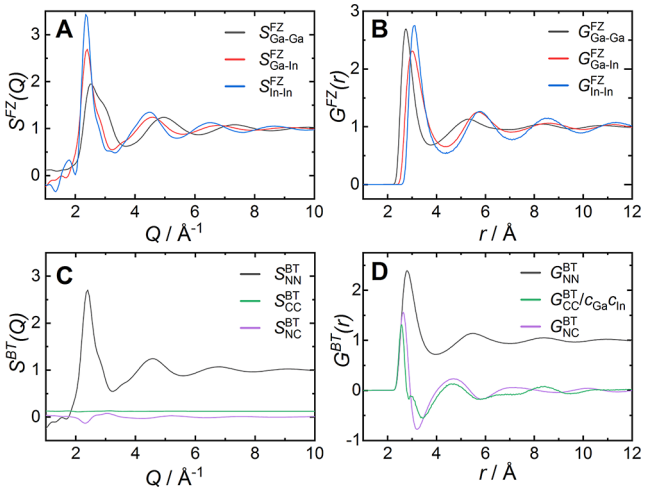

Figure 5. Partial structure factors and corresponding partial pair distribution functions obtained from the final EPSR model of $Ga_{0.858}In_{0.142}$ at T = 150 °C. Panels A, B: Faber−Ziman structure factors $S(Q)^{FZ}$ and pair distribution functions $G(r)^{FZ}$. Panels C, D: Bhatia-Thornton structure factors $S(Q)^{BT}$ and pair distribution functions $G(r)^{BT}$. $G_{CC}{}^{BT}$ is normalized by $c_{Ga}c_{In}$ for better visibility.

the Faber−Ziman structure factors shows that the first peak of the gallium−gallium partial structure factor $S^{FZ}_{GaGa(Q)}$ has a clear double peak structure (Figure 5A) and is responsible for the high-Q shoulder in the total structure factor $S(Q)$. On the contrary, $S^{FZ}_{InIn(Q)}$ is close to a hard sphere-like structure factor. The corresponding Faber−Ziman pair distribution functions $G^{FZ}_{GaGa(r)}$, $G^{FZ}_{GaIn(r)}$ $G^{FZ}_{InIn(r)}$ show sharp peaks at r = 2.76 Å, r = 3.00 Å and r = 3.09 Å, respectively, corresponding to the distances between atom pairs within the first coordination shell. Both $S^{FZ}_{GaIn(Q)}$ and $G^{FZ}_{GaIn(r)}$ resemble closely the indium−indium partial contributions, while the gallium−gallium contributions appear dissimilar.

The derived Bhatia−Thornton structure factors $S^{BT}_{NN(Q)}$, $S^{BT}_{NC(Q)}$, $S^{BT}_{CC(Q)}$ give the number−number, number−concentration and concentration−concentration correlations in the eutectic $Ga_{0.858}In_{0.142}$ alloy, respectively (Figure 5C).[64,65] $S^{BT}_{CC(Q)}$ shows only small oscillations around the high-Q limit of $c_{Ga}c_{In}$ = 0.122, indicating negligible chemical order in liquid $Ga_{0.858}In_{0.142}$. Similarly, $S^{BT}_{NC(Q)}$ shows only small deviations from zero. Hence, $S^{BT}_{NN(Q)}$ is the main contribution to the total $S(Q)$ and topological short-range order is prominent in liquid $Ga_{0.858}In_{0.142}$. Also in real space, $G^{BT}_{NN(r)}$ is the main contribution to the total pair distribution function $G(r)$ and closely follows the overall pair distribution function. The functions $G^{BT}_{NN(r)}$ describing the chemical order and $G^{BT}_{NC(r)}$ describing the correlation between density and concentration fluctuations show rapid small oscillations, with an approximately doubled frequency compared to $G^{BT}_{NN(r)}$. These small rapid oscillations can be ascribed to size effects and are typically present for solutions containing atoms of significantly different diameters.

Integration of the partial radial distribution functions $T^j_i(r) = 4\pi\, c_j\, \rho_0\, r^2\, G^{FZ}_{ij(r)}$ up to the first minimum yields the partial coordination numbers CN^j_i for atoms of type j around atoms of type i in the first coordination shell. The values for liquid $Ga_{0.858}In_{0.142}$ at T = 150 °C are CN^{Ga}_{Ga} = 8.5(1), CN^{In}_{Ga} = 2.1(2), CN^{Ga}_{In} = 12.5(1) and CN^{In}_{In} = 2.0(4). The corresponding Warren-Cowley short-range order parameter for the first coordination shell α_{WC} = −0.04 is close to the value for a statistical distribution (α_{WC} = 0).[66] The absence of strong interactions, e.g., due to charge transfer between Ga and In, is in line with constant atomic volumes across the composition series, as evidenced by the negligible molar excess volumes (cf. Figure 1C).

CONCLUSIONS

Neutron diffraction data and EPSR simulation results on liquid gallium at 150 °C have provided experimental support for the hypothesis that the high-Q shoulder observed on the first diffraction peak does not originate from gallium dimers in the melt, but rather from structural rearrangements in the second coordination shell. The empirical potential U^{EP} refined for Ga from EPSR simulations qualitatively resembles the results expected for an ordering induced by Friedel oscillations;[9] however, quantitatively, the oscillation period does not match well with theoretical predictions.

Analysis of short-range order in the eutectic alloy $Ga_{0.858}In_{0.142}$ did not indicate a strong preference for hetero- or homo-atomic interactions, as evidenced by inconspicuous behavior of $S^{BT}_{CC(Q)}$ and a near-zero Warren-Cowley order parameter. The absence of strong chemical interactions, such as charge transfer, is also evidenced by the constant atomic volumes across the composition range.

EPSR analysis at the eutectic composition suggests a particularly deep minimum in the pair potential $U^{LJ+EP}_{GaIn(r)}$ which could originate from a maximum in packing density as observed for unequal hard spheres around 20% fraction of the larger spheres.[67] An inflection point in the liquidus curve around the equiatomic composition had also been observed in the Ag−Sn system and was suggested as a composition with particularly difficult packing of unequal atoms. Similarly to the

https://doi.org/10.1021/acs.jpcc.3c03857
J. Phys. Chem. C 2023, 127, 16687−16694

results of Gebhardt, the presence of two types of incompatible coordination environments or cluster types was postulated.[46,47]

Extrapolating from the detailed analysis of the eutectic alloy to the In-rich compositions, preferred interactions between atom pairs may be excluded as cause for the reported positive enthalpy of mixing ΔH_M in this system. In line with the symmetric curve of $\Delta H_M(x)$, also valence effects can be excluded for alloys of these isoelectronic elements. While the measured partial atomic volumes are constant across the composition series, the volumetric density and therefore also density of the electron gas in the liquid alloys is increased relative to the elemental densities. Similar to the binary alkali metal alloys, the observed positive mixing enthalpy in Ga−In alloys can therefore be related to electronic effects, as the charge density is modified from the equilibrium values of the elemental end members.[68,69]

The results collected from volumetric density and diffraction data across the composition series, as well as EPSR simulations for liquid Ga and liquid $Ga_{0.858}In_{0.142}$, corroborate that the structure of liquid gallium has anomalous features compared to simple hard-sphere liquids, which manifest in a redistribution of Ga atoms from the first to the second coordination sphere, leading to an observable high-Q shoulder in diffraction data. Determining the reason for this anomalous behavior will require additional studies. Binary Ga−In alloys, on the other hand, show no indication of preferred atomic interactions in trends of molar excess volumes or analysis of chemical short-range order. Mixing with indium appears to "dilute" the anomalous properties of liquid Ga and especially on the indium-rich side the effect of Ga on the diffraction data (high-Q shoulder) vanishes.

■ ASSOCIATED CONTENT

Supporting Information

The Supporting Information is available free of charge at https://pubs.acs.org/doi/10.1021/acs.jpcc.3c03857.

Additional figures on density measurements, diffraction data analysis, and interatomic potentials; table of measured density values (PDF)

■ AUTHOR INFORMATION

Corresponding Author

Alfred Amon − *Department of Chemistry, University College London, London WC1H 0AJ, U.K.; Material Science Division, Lawrence Livermore National Laboratory, Livermore, California 94550, United States;* orcid.org/0000-0002-5301-8867; Email: amon1@llnl.gov

Authors

Philip A. Chater − *Diamond Light Source Ltd., Didcot OX11 0DE, U.K.;* orcid.org/0000-0002-5513-9400

Gavin Vaughan − *European Synchrotron Radiation Facility, Grenoble Cedex 9 F-38043, France*

Rachael Smith − *Department of Chemistry, University College London, London WC1H 0AJ, U.K.*

Christoph G. Salzmann − *Department of Chemistry, University College London, London WC1H 0AJ, U.K.*

Complete contact information is available at: https://pubs.acs.org/10.1021/acs.jpcc.3c03857

Author Contributions

A.A. wrote the manuscript and performed physical experiments and data evaluation. A.A. and R.S. performed neutron scattering experiments. P.C. and G.V. performed X-ray scattering experiments. A.A. and C.G.S. developed the concept for this study. All authors have given approval to the final version of the manuscript.

Funding

Open Access is funded by the Austrian Science Fund (FWF).

Funding

The authors are grateful for financial support with a Schrödinger fellowship (A.A.) by the Austrian Science Fund (FWF): J4325, and to RAL-ISIS (UK) and the ESRF (France) for granting beamline access. This study was performed under the auspices of the U.S. Department of Energy by Lawrence Livermore National Laboratory under Contract DE-AC52-07NA27344.

Notes

The authors declare no competing financial interest.

■ ACKNOWLEDGMENTS

A.A. is grateful to Alex Hannon (GEM, RAL-ISIS) for support during neutron scattering experiments.

■ REFERENCES

(1) Gong, X. G.; Chiarotti, G. L.; Parrinello, M.; Tosatti, E. α-gallium: A metallic molecular crystal. *Phys. Rev. B: Condens. Matter Mater. Phys.* **1991**, *43*, 14277−14280.

(2) Fischer, D.; Andriyevsky, B.; Schön, J. C. Systematics of the allotrope formation in elemental gallium films. *Mater. Res. Express* **2019**, *6*, 116401.

(3) Köster, H.; Hensel, F.; Franck, E. U. Dichte, Kompressibilität und thermische Ausdehnung des flüssigen Galliums bis 600 °C und 2500 bar. *Z. Phys. Chem.* **1970**, *74*, 43−46.

(4) Hoyer, W.; Thomas, E.; Wobst, M. Structure investigation on liquid gallium. *Krist. Tech.* **1980**, *15*, 903−910.

(5) Gong, X. G.; Chiarotti, G. L.; Parrinello, M.; Tosatti, E. Coexistence of Monatomic and Diatomic Molecular Fluid Character in Liquid Gallium. *Europhys. Lett.* **1993**, *21*, 469−475.

(6) Chen, L.-Y.; Tang, P.-H.; Wu, T.-M. Analysis of local bond-orientational order for liquid gallium at ambient pressure: Two types of cluster structures. *J. Chem. Phys.* **2016**, *145*, 024506.

(7) Tsay, S.-F.; Wang, S. Anomalies in the liquid structure of Ga metal. *Phys. Rev. B: Condens. Matter Mater. Phys.* **1994**, *50*, 108−112.

(8) Niu, H.; Bonati, L.; Piaggi, P. M.; Parrinello, M. Ab initio phase diagram and nucleation of gallium. *Nat. Commun.* **2020**, *11*, 2654.

(9) Tsai, K. H.; Wu, T.-M.; Tsay, S.-F. Revisiting anomalous structures in liquid Ga. *J. Chem. Phys.* **2010**, *132*, 034502.

(10) Mokshin, A. V.; Khusnutdinoff, R. M.; Galimzyanov, B. N.; Brazhkin, V. V. Extended short-range order determines the overall structure of liquid gallium. *Phys. Chem. Chem. Phys.* **2020**, *22*, 4122−4129.

(11) Bererhi, A.; Bosio, L.; Cortès, R. X-ray diffraction study on amorphous gallium. *J. Non-Cryst. Solids* **1979**, *30*, 253−262.

(12) Daeneke, T.; Khoshmanesh, K.; Mahmood, N.; de Castro, I. A.; Esrafilzadeh, D.; Barrow, S. J.; Dickey, M. D.; Kalantar-zadeh, K. Liquid metals: fundamentals and applications in chemistry. *Chem. Soc. Rev.* **2018**, *47*, 4073−4111.

(13) Esrafilzadeh, D.; Zavabeti, A.; Jalili, R.; Atkin, P.; Choi, J.; Carey, B. J.; Brkljača, R.; O'Mullane, A. P.; Dickey, M. D.; Officer, D. L.; et al. Room temperature CO 2 reduction to solid carbon species on liquid metals featuring atomically thin ceria interfaces. *Nat. Commun.* **2019**, *10*, 865.

(14) Hou, Y.; Wang, F.; Qin, C.; Wu, S.; Cao, M.; Yang, P.; Huang, L.; Wu, Y. A self-healing electrocatalytic system via electro-

hydrodynamics induced evolution in liquid metal. *Nat. Commun.* **2022**, *13*, 7625.
(15) Taccardi, N.; Grabau, M.; Debuschewitz, J.; Distaso, M.; Brandl, M.; Hock, R.; Maier, F.; Papp, C.; Erhard, J.; Neiss, C.; et al. Gallium-rich Pd−Ga phases as supported liquid metal catalysts. *Nat. Chem.* **2017**, *9*, 862−867.
(16) Kochat, V.; Samanta, A.; Zhang, Y.; Bhowmick, S.; Manimunda, P.; Asif, S. A. S.; Stender, A. S.; Vajtai, R.; Singh, A. K.; Tiwary, C. S.; Ajayan, P. M. Atomically thin gallium layers from solid-melt exfoliation. *Sci. Adv.* **2018**, *4*, No. e1701373.
(17) Idrus-Saidi, S. A.; Tang, J.; Lambie, S.; Han, J.; Mayyas, M.; Ghasemian, M. B.; Allioux, F.-M.; Cai, S.; Koshy, P.; Mostaghimi, P.; Steenbergen, K. G.; Barnard, A. S.; Daeneke, T.; Gaston, N.; Kalantar-Zadeh, K. Liquid metal synthesis solvents for metallic crystals. *Science* **2022**, *378*, 1118−1124.
(18) Wang, K.; Jiang, K.; Chung, B.; Ouchi, T.; Burke, P. J.; Boysen, D. A.; Bradwell, D. J.; Kim, H.; Muecke, U.; Sadoway, D. R. Lithium-antimony-lead liquid metal battery for grid-level energy storage. *Nature* **2014**, *514*, 348−350.
(19) Jin, Y.; Liu, K.; Lang, J.; Zhuo, D.; Huang, Z.; Wang, C.; Wu, H.; Cui, Y. An intermediate temperature garnet-type solid electrolyte-based molten lithium battery for grid energy storage. *Nat. Energy* **2018**, *3*, 732−738.
(20) Tabatabai, A.; Fassler, A.; Usiak, C.; Majidi, C. Liquid-Phase Gallium−Indium Alloy Electronics with Microcontact Printing. *Langmuir* **2013**, *29*, 6194−6200.
(21) Zheng, Y.; He, Z.-Z.; Yang, J.; Liu, J. Personal electronics printing via tapping mode composite liquid metal ink delivery and adhesion mechanism. *Sci. Rep.* **2014**, *4*, 4588.
(22) Khoshmanesh, K.; Tang, S.-Y.; Zhu, J. Y.; Schaefer, S.; Mitchell, A.; Kalantar-zadeh, K.; Dickey, M. D. Liquid metal enabled microfluidics. *Lab Chip* **2017**, *17*, 974−993.
(23) Conner, C.; de Visser, T.; Loessberg, J.; Sherman, S.; Smith, A.; Ma, S.; Napoli, M. T.; Pennathur, S.; Weld, D. Energy Harvesting with a Liquid-Metal Microfluidic Influence Machine. *Phys. Rev. Appl.* **2018**, *9*, 044008.
(24) Yu, Z.; Chen, Y.; Yun, F. F.; Cortie, D.; Jiang, L.; Wang, X. Discovery of a Voltage-Stimulated Heartbeat Effect in Droplets of Liquid Gallium. *Phys. Rev. Lett.* **2018**, *121*, 024302.
(25) Cole, T.; Tang, S.-Y. Liquid metals as soft electromechanical actuators. *Mater. Adv.* **2022**, *3*, 173−185.
(26) Wang, Q.; Pan, C.; Zhang, Y.; Peng, L.; Chen, Z.; Majidi, C.; Jiang, L. Magnetoactive liquid-solid phase transitional matter. *Matter* **2023**, *6*, 855−872.
(27) Di Cicco, A. Phase Transitions in Confined Gallium Droplets. *Phys. Rev. Lett.* **1998**, *81*, 2942−2945.
(28) Gebhardt, B.; Halm, T.; Hoyer, W. The structure of liquid Ga-In alloys. *J. Non-Cryst. Solids* **1995**, *192−193*, 306−308.
(29) Ding, G.-H.; Li, X.-Y.; Huang, Z.-Y.; Li, M. Structural order and anomaly of liquid gallium-indium during isothermal dissolution of indium in liquid gallium. *Phys. Chem. Liq.* **2013**, *51*, 255−260.
(30) Yu, Q.; Ahmad, A. S.; Ståhl, K.; Wang, X. D.; Su, Y.; Glazyrin, K.; Liermann, H. P.; Franz, H.; Cao, Q. P.; Zhang, D. X.; et al. Pressure-induced structural change in liquid GaIn eutectic alloy. *Sci. Rep.* **2017**, *7*, 1139.
(31) Yu, Q.; Su, Y.; Wang, X. D.; Ståhl, K.; Glazyrin, K.; Liermann, H. P.; Franz, H.; Cao, Q. P.; Zhang, D. X.; Jiang, J. Z. Structural evolution in liquid GaIn eutectic alloy under high temperature and pressure. *J. Appl. Phys.* **2019**, *126*, 015902.
(32) Yu, Q.; Wang, X. D.; Su, Y.; Cao, Q. P.; Ren, Y.; Zhang, D. X.; Jiang, J. Z. Liquid-to-liquid crossover in the GaIn eutectic alloy. *Phys. Rev. B: Condens. Matter Mater. Phys.* **2017**, *95*, 224203.
(33) Zhao, X.; Bian, X.; Bai, Y.; Li, X. Structure and fragility of supercooled Ga-In melts. *J. Appl. Phys.* **2012**, *111*, 103514.
(34) Zhao, X.; Bian, X.; Qin, J.; Liu, Y.; Bai, Y.; Li, X.; Feng, L.; Zhang, K.; Yang, C. Unusual coordination structure in undercooled eutectic Ga-In alloy melt. *Europhys. Lett.* **2014**, *107*, 36004.
(35) Anderson, T. J.; Ansara, I. The Ga-In (Gallium-Indium) System. *J. Phase Equil.* **1991**, *12*, 64−72.
(36) Rao, M. V.; Tiller, W. A. The system In-Ga: Thermodynamics and computed phase equilibria. *J. Mater. Sci.* **1972**, *7*, 14−18.
(37) Yu, S.; Kaviany, M. Electrical, thermal, and species transport properties of liquid eutectic Ga-In and Ga-In-Sn from first principles. *J. Chem. Phys.* **2014**, *140*, 064303.
(38) Plevachuk, Y.; Sklyarchuk, V.; Eckert, S.; Gerbeth, G.; Novakovic, R. Thermophysical Properties of the Liquid Ga-In-Sn Eutectic Alloy. *J. Chem. Eng. Data* **2014**, *59*, 757−763.
(39) Ben Shalom, S.; Kim, H. G.; Emuna, M.; Argaman, U.; Greenberg, Y.; Lee, J.; Yahel, E.; Makov, G. Anomalous pressure dependent phase diagram of liquid Ga−In alloys. *J. Alloys Compd.* **2020**, *822*, 153537.
(40) Bros, J.-P. Enthalpies of formation of the ternary liquid alloys gallium-indium (french title: Enthalpies de Formation des Alliages Liquides gallium-Indium). *Comptes Rendus Acad. Sci.* **1966**, *263*, 977−980.
(41) Bros, J.-P.; Castanet, R.; Laffitte, M. Mixing enthalpy of the liquid alloys gallium-indium at 469 °C (french title : Enthalpie de melange des alliages liquides gallium-indium a 469C). *Comptes Rendus Acad. Sci.* **1967**, *264*, 1804−1806.
(42) Pong, R.; Donaghey, L. F. Thermodynamic studies of gallium-indium liquid alloys by solid state electrochemistry with oxide electrolytes. *J. Chem. Eng. Data* **1976**, *21*, 370−374.
(43) Macur, G. J.; Edwards, R. K.; Wahlbeck, P. G. Measurement of activities in gallium-indium liquid alloys. *J. Phys. Chem.* **1968**, *72*, 1047−1050.
(44) Svirbely, W. J.; Read, S. M. The thermodynamic properties of liquid ternary zinc, indium and gallium solutions. *J. Phys. Chem.* **1962**, *66*, 658−662.
(45) William Hume, R. Miscibility and Primary Solid Solutions in Alloys. In *Electrons At. Met. Alloys*, 2nd ed.; Ilife & Sons: London, 1948; p 273.
(46) Wilson, J. R. The Structure of Liquid Metals and Alloys. *Metall. Rev.* **1965**, *10*, 381−590.
(47) Oriani, R. A. Thermodynamics of liquid Ag-Au and Au-Cu alloys and the question of strain energy in solid solutions. *Acta Metall* **1956**, *4*, 15−25.
(48) Köster, H.; Hensel, F.; Franck, E. Dichte, Kompressibilität und thermische Ausdehnung des flüssigen Galliums bis 600 °C und 2500 bar. *Ber. Bunsengesellschaft Z. Phys. Chem.* **1970**, *74*, 43.
(49) Zen, E. Validity of vegard's law. *Am. Mineral.* **1956**, *41*, 523−524.
(50) Sears, V. F. Neutron scattering lengths and cross sections. *Neutron News* **1992**, *3*, 26−37.
(51) Pauling, L. Atomic Radii and Interatomic Distances in Metals. *J. Am. Chem. Soc.* **1947**, *69*, 542−553.
(52) Price, D. L.; Moss, S. C.; Reijers, R.; Saboungi, M.-L.; Susman, S. Intermediate-range order in glasses and liquids. *J. Phys. Condens. Matter* **1989**, *1*, 1005−1008.
(53) Saboungi, M.; Geertsma, W.; Price, D. L. Ordering in Liquid Alloys. *Annu. Rev. Phys. Chem.* **1990**, *41*, 207−244.
(54) Vahvaselkä, K. S. Total and Partial Interference Functions, Radial Atomic Distributions, and Electrical Resistivities for Liquid Indium and Liquid Gallium-Indium Alloys. *Phys. Status Solidi A* **1982**, *72*, 261−271.
(55) Soper, A. K. Empirical potential Monte Carlo simulation of fluid structure. *Chem. Phys.* **1996**, *202*, 295−306.
(56) Soper, A. K. Partial structure factors from disordered materials diffraction data: An approach using empirical potential structure refinement. *Phys. Rev. B: Condens. Matter Mater. Phys.* **2005**, *72*, 104204.
(57) Blandin, A.; Daniel, E.; Friedel, J. On the knight shift of alloys. *Philos. Mag. J. Theor. Exp. Appl. Phys.* **1959**, *4*, 180−182.
(58) Lindhard, J. On the properties of a gas of charged particles. *Det Kongelige Danske Videnskabernes Selskab*; University of Copenhagen, 1954; Vol. *28*.
(59) March, N. H. Electron screening and effective ion-ion interactions. In *Liquid Metal Concepts Theory*; Cambridge University Press, 1968; p 26.

https://doi.org/10.1021/acs.jpcc.3c03857
J. Phys. Chem. C 2023, 127, 16687−16694

(60) Faber, T. E. Potentials and Pseudo-Potentials. In *Introduction Theory Liquid Metals*; Cambridge University Press, 1972; p 28.
(61) Percus, J. K.; Yevick, G. J. Analysis of Classical Statistical Mechanics by Means of Collective Coordinates. *Phys. Rev.* **1958**, *110*, 1−13.
(62) Percus, J. K. Approximation Methods in Classical Statistical Mechanics. *Phys. Rev. Lett.* **1962**, *8*, 462−463.
(63) Gray, C. G.; Gubbins, K. E. *Theory of Molecular Fluids: I: Fundamentals*; Oxford University Press: Oxford, 1984.
(64) Bhatia, A. B.; Thornton, D. E. Structural Aspects of the Electrical Resistivity of Binary Alloys. *Phys. Rev. B: Condens. Matter Mater. Phys.* **1970**, *2*, 3004−3012.
(65) Salmon, P. S. Moments of the Bhatia−Thornton partial pair-distribution functions. *J. Phys. Condens. Matter* **2005**, *17*, S3537−S3542.
(66) Cowley, J. M. An Approximate Theory of Order in Alloys. *Phys. Rev.* **1950**, *77*, 669−675.
(67) Santiso, E.; Müller, E. A. Dense packing of binary and polydisperse hard spheres. *Mol. Phys.* **2002**, *100*, 2461−2469.
(68) Yokokawa, T.; Kleppa, O. J. Heats of Mixing in Binary-Liquid—Alkali-Metal Mixtures. *J. Chem. Phys.* **1964**, *40*, 46−54.
(69) Kleppa, O. J. Aspects of the thermodynamics of metallic solutions. *J. Phys. Radium* **1962**, *23*, 763−772.
(70) Vaughan, G. B. M.; Baker, R.; Barret, R.; Bonnefoy, J.; Buslaps, T.; Checchia, S.; Duran, D.; Fihman, F.; Got, P.; Kieffer, J.; et al. ID15A at the ESRF − a beamline for high speed operando X-ray diffraction, diffraction tomography and total scattering. *J. Synchrotron Radiat.* **2020**, *27*, 515−528.
(71) Filik, J.; Ashton, A. W.; Chang, P. C. Y.; Chater, P. A.; Day, S. J.; Drakopoulos, M.; Gerring, M. W.; Hart, M. L.; Magdysyuk, O. V.; Michalik, S.; et al. Processing two-dimensional X-ray diffraction and small-angle scattering data in DAWN 2. *J. Appl. Crystallogr.* **2017**, *50*, 959−966.
(72) McLain, S. E.; Bowron, D. T.; Hannon, A. C.; Soper, A. K. *GUDRUN, a Computer Program Developed for Analysis of Neutron Diffraction Data, ISIS Facility*; Rutherford Appleton Laboratory: Chilton, UK, 2012.
(73) McDaniel, B. D. Slow Neutron Resonances in Indium. *Phys. Rev.* **1946**, *70*, 832−841.
(74) Amon, A.; Sener, M. E.; Rosu-Finsen, A.; Hannon, A. C.; Slater, B.; Salzmann, C. G. Preparation and Structure of the Ion-Conducting Mixed Molecular Glass Ga2I3.17. *Inorg. Chem.* **2021**, *60*, 6319−6326.

https://doi.org/10.1021/acs.jpcc.3c03857
J. Phys. Chem. C 2023, 127, 16687−16694